ADVANCED MATERIALS
www.advmat.de

Active Micro-Actuators for Optical Modulation Based on a Planar Sliding Triboelectric Nanogenerator

*Chi Zhang, Wei Tang, Yaokun Pang, Changbao Han, and Zhong Lin Wang**

With the development of micro/nano electromechanical systems (MEMS/NEMS), local power supplies have become especially important for their applications in human health, infrastructure, environmental aspects, and sensor network monitoring.[1] Because of their disadvantages, such as their unsustainability, environmental pollution, and high resource consumption, batteries cannot meet the growing demands of the MEMS/NEMS technology and sensor network environments. Sustainable and self-powered technology by the scavenging of ambient mechanical energy would be a great solution and future trend.[2,3] Based on micro/nano processing technology, various energy-harvesting technologies for micro/nano systems have been studied, such as electrostatic,[4] piezoelectric,[5] electromagnetic,[6] and magnetostriction.[7]

Recently, the invention of a triboelectric nanogenerator (TENG) has provided an effective approach to convert ambient mechanical energy into electricity.[8–14] The working principle of the TENG is based on the coupling of contact electrification and electrostatic induction. The performance of TENGs has been improved by orders of magnitude since their invention in 2011,[15] and they have been validated to be equally important to traditional electromagnetic induction generators for power generation by systematic theoretical and experimental comparison.[16,17] So far, TENGs have been applied to drive microelectronic devices, such as LEDs,[18] wireless transmitters,[19] and thermometers,[20,21] but not for micro/nano-mechanical or MEMS/NEMS devices. Because of their continuously improving performances and their high output voltages, TENGs are very suitable for tuning/controlling the capacitor voltage in certain devices, such as tribotronic and triboelectric UV emission devices,[22,23] and they could also be used to drive/control capacitive micro-actuators.

In this work, we report the development of a planar sliding TENG with dual-output voltages that can independently characterize the displacements of the triboelectric-layer in the *X* and *Y* directions, respectively. Based on this planar sliding TENG an active piezoelectric micro-actuator and an active electrostatic MEMS actuator were developed for optical modulation. Owing to the high-voltage, dual-channel outputs the micro-actuators were driven by the planar sliding TENG and their optical direction and power could be modulated by the external mechanical energy. The active micro-actuators based on this TENG could open up the road to more important potential applications of independent and sustainable self-powered MEMS/NEMS.

The basic structure of the planar sliding TENG is composed of a freestanding triboelectric-layer and two pairs of orthogonal electrodes, as schematically illustrated in **Figure 1**a. For the fabrication of the planar sliding TENG device, Al and polytetrafluoroethylene (PTFE), with a large difference in triboelectric polarity, were selected as the conducting film and the freestanding triboelectric layer, respectively. Two rectangular Al films, each tailored to 7 cm × 14 cm, were deposited side by side on the bottom acrylic substrate with a 0.1 cm gap in the *X* direction in between them, and they served as the bottom electrodes. Two more rectangular Al films of the same size were deposited side by side on the top acrylic substrate, this time with a 0.1 cm gap in the *Y* direction in between them, and they served as the top electrodes. Two square PTFE films, each tailored to 7 cm × 7 cm, were then adhered on both sides of the supporting acrylic substrate of the same size and each was brought into close contact with either the top or bottom electrode.

In order to further improve the triboelectric charge density, the surface of both PTFE films was treated by inductively coupled plasma (ICP) to create nanoparticle structures, as shown in Figure 1b. Driven by a planar force, the freestanding PTFE layer could slide in the plane between the top and bottom electrodes, through which dual-channel output voltages were supplied.

When the PTFE layer slides in plane rubbing against the Al electrodes, the triboelectric effect will render the PTFE surface with negative charges, and the Al electrodes with positive charges. Figure 1c shows the working principle of the planar sliding TENG if the PTFE layer slides in the *X* direction. In the original state (Figure 1c<i>), the PTFE layer is at a position where it fully overlaps with the left bottom electrode. All the positive charges in the electrode will be attracted to the upper surface of the bottom electrode and there is no potential difference between the two bottom electrodes. Then, when the PTFE layer slides in the *X* direction (Figure 1c<ii>), some of the positive charges will lose their constraints and will have a tendency to flow from the left bottom electrode to the right one. The potential difference between them will increase with the sliding distance in the *X* direction. When the PTFE square completely overlaps with the right bottom electrode (Figure 1c<iii>), all of the positive charges on the left hand side will have lost their constraint and the potential difference will have reached its maximal value. Subsequently, a backward sliding of the PTFE layer in the *X* direction will attract the positive charges again and decrease the potential difference

Dr. C. Zhang, Dr. W. Tang, Y. K. Pang, Dr. C. B. Han, Prof. Z. L. Wang
Beijing Institute of Nanoenergy and Nanosystems
Chinese Academy of Sciences
Beijing 100083, P.R. China
E-mail: zlwang@gatech.edu
Prof. Z. L. Wang
School of Material Science and Engineering
Georgia Institute of Technology
Atlanta, Georgia 30332–0245, United States

DOI: 10.1002/adma.201404291

 © 2014 WILEY-VCH Verlag GmbH & Co. KGaA, Weinheim

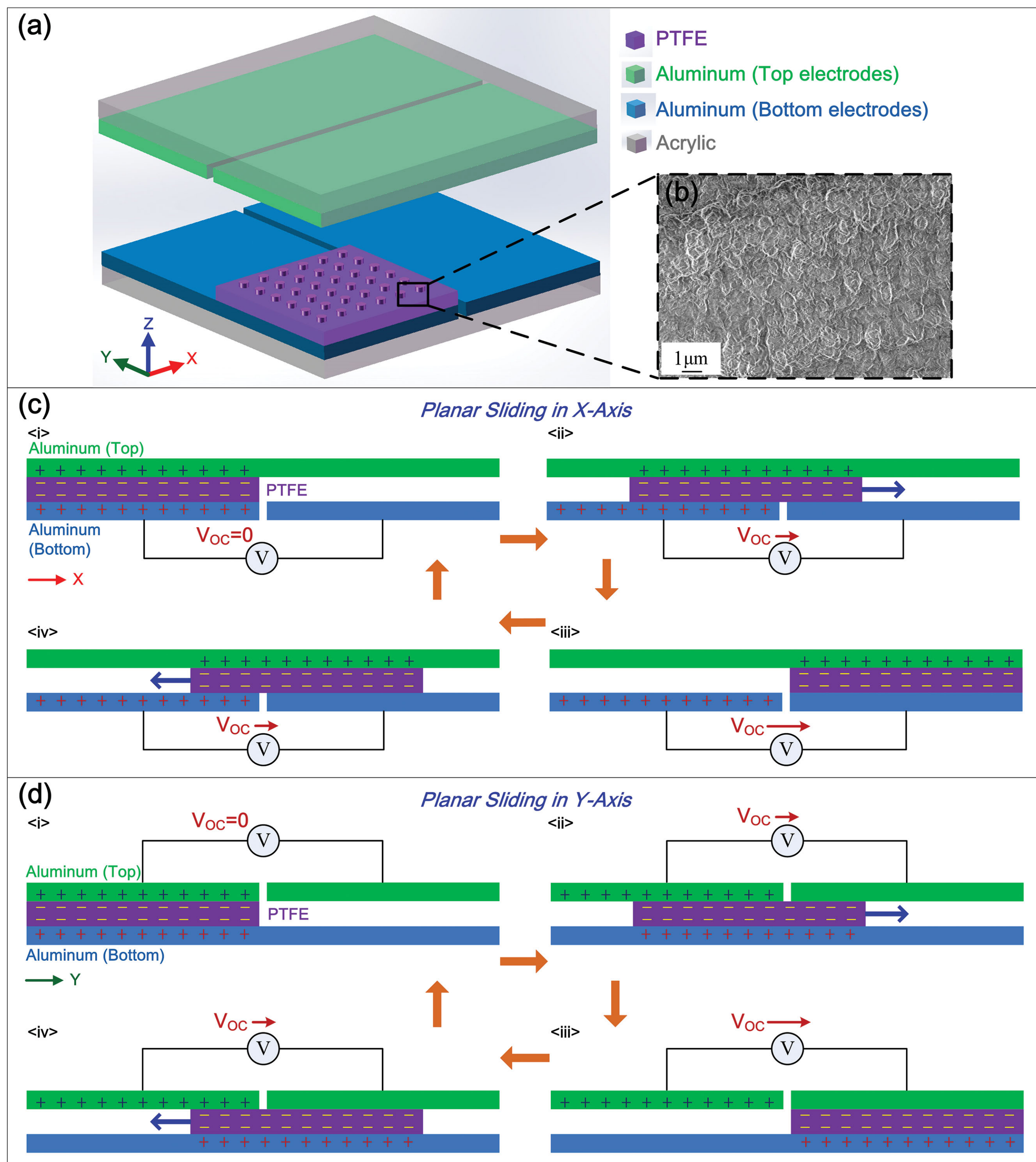

Figure 1. Device structure and working principles of the planar sliding triboelectric nanogenerator (TENG). a) Structural design drawing of the planar sliding TENG with two pairs of orthogonal electrodes. b) SEM image of PTFE nanoparticles on the surface of the PTFE film. c) Schematic working principle of the planar sliding TENG when the PTFE layer slides in the *X* direction. d) Schematic working principle of the planar sliding TENG when the PTFE layer slides in the *Y* direction.

(Figure 1c<iv>), until returning to the original state. During the whole process, the upper surface of the PTFE layer slides against the top electrode at the same time. Because all of the positive charges in the top electrode will be attracted to the lower surface by the PTFE layer, the potential difference between the two top electrodes will not be changed by sliding in the *X* direction.

When the PTFE layer slides in the *Y* direction, the working principle of the planar sliding TENG is illustrated in Figure 1d. Again, when the PTFE layer is at the position

© 2014 WILEY-VCH Verlag GmbH & Co. KGaA, Weinheim

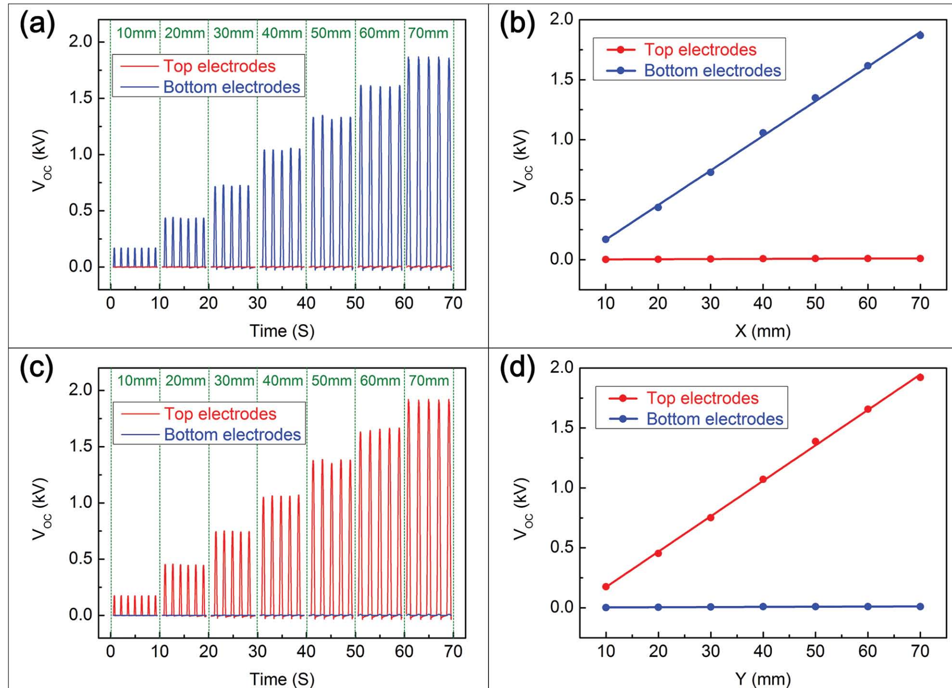

Figure 2. Influence of the sliding displacement on the output voltages. a,c) The open-circuit voltages (V_{OC}) when the PTFE layer slides in the *X* and *Y* direction, respectively, for 7 different sliding displacements from 10 to 70 mm at an acceleration rate of ±1 m s^{-2}. b,d) The relationship between V_{OC} and the displacements in the *X* and *Y* direction. The sensitivity was 28.9 V mm^{-1} for the *X* direction and 29.6 V mm^{-1} for the *Y* direction.

where it fully overlaps with the left top electrode in the original state (Figure 1d<i>), there will be no potential difference between the two top electrodes. When the PTFE layer slides in the *Y* direction (Figure 1d<ii>), the potential difference will increase with the sliding distance in the *Y* direction, and reach its maximal value when the PTFE overlaps fully with the top right electrode (Figure 1d<iii>). Also, a backward sliding of the PTFE layer in the *Y* direction decreases the potential difference (Figure 1d<iv>) until returning to the original state. Although the lower surface of the PTFE layer simultaneously slides against the bottom electrode in the whole process, the potential difference between the two bottom electrodes does not change by sliding in the *Y* direction. Therefore, when the PTFE layer slides in plane, the displacements in the *X* and *Y* directions are independently characterized by the dual-output voltages.

The dual-channel open-circuit voltages (V_{OC}) when the PTFE layer slides in the *X* and *Y* directions were measured as shown in **Figure 2**a,c, respectively, for 7 different sliding displacements from 10 to 70 mm at an acceleration rate of ±1 m s^{-2}. The V_{OC} of the bottom and top electrodes have linear relationships to the sliding displacement in the *X* and *Y* direction, respectively, as shown in Figure 2b,d. The sensitivity was 28.9 V mm^{-1} for the *X* direction and 29.6 V mm^{-1} for the *Y* direction. Figure 2b,d shows that the bottom and top electrodes have almost no output voltages when the PTFE layer slides in the *Y* and *X* directions, respectively, because the PTFE layer is always in its original state (Figures 1c<i> and 1d<i>) in the direction that is perpendicular to the sliding direction. The measurement results are in accordance with the structural design and working principle, which can linearly and independently represent the planar sliding.

Figure 3a,c shows the measured dual-channel V_{OC} when the PTFE layer slides in the *X* and *Y* direction, respectively, for 6 different sliding accelerations (which correspond to different maximum velocities) from 0.1 to 1 m s^{-2} at a sliding displacement of 70 mm. The maximal V_{OC} of both the bottom and top electrodes were almost constant with increasing sliding speeds, which is shown in Figure 3b,d. Though a slight increase was found at high speed, which may result from the relatively increased triboelectric charge density of the PTFE surface, the overall consensus is that the sliding speed has little influence on the dual-channel output voltages of around 1.83 kV and 1.85 kV, respectively.

Because of the high output voltages the planar sliding TENG can be used to actuate capacitive devices. The relationships between the dual-channel applied voltages U_b and U_t and the load capacitance C_{load} were analyzed using Gauss' Theorem in the Supporting Information, which can be described by:

$$U_b = \frac{Q \cdot L_x}{(C_0 + C_{load}) \cdot L} \tag{1}$$

$$U_t = \frac{Q \cdot L_y}{(C_0 + C_{load}) \cdot L} \tag{2}$$

where *Q* is the triboelectric charge quantity on each side of the PTFE surface, *L* is the side length of the PTFE layer, L_x and L_y are the sliding distances to the original positions in the *X* and *Y* directions, respectively, and C_0 is the capacitance between the two bottom electrodes, which is also the capacitance between the two top electrodes for the symmetric structures. Therefore,

© 2014 WILEY-VCH Verlag GmbH & Co. KGaA, Weinheim

COMMUNICATION

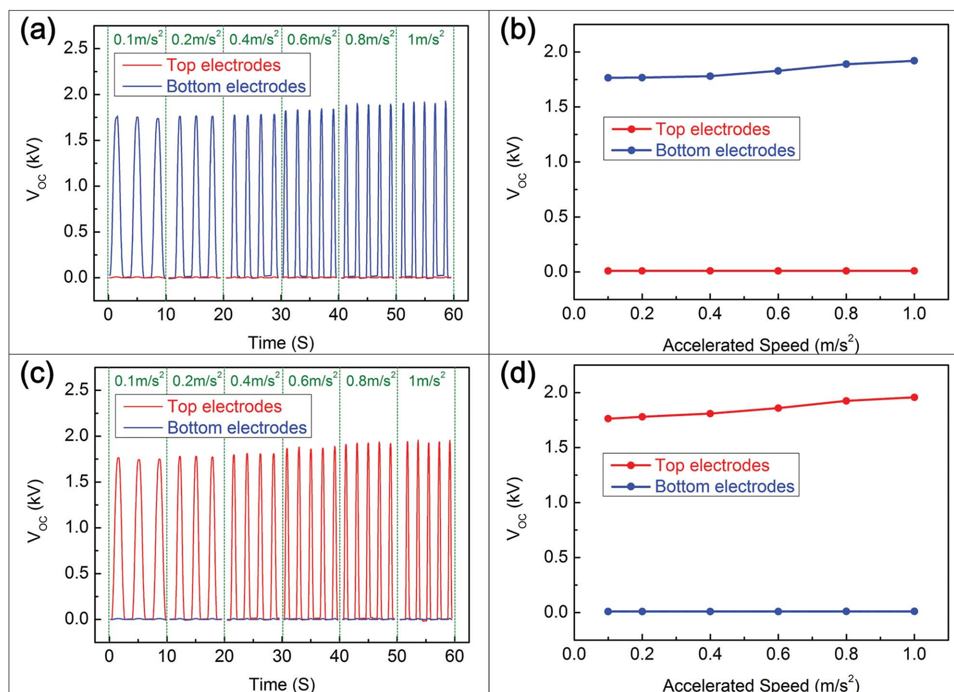

Figure 3. Influence of the sliding speeds (acceleration) on the output voltages. a,c) The open-circuit voltage (V_{OC}) when the PTFE layer slides in the X and Y direction, respectively, at 6 different sliding accelerations (which correspond to different maximum velocities) from 0.1 to 1 m s^{-2} at a sliding displacement of 70 mm. b,d) The relationship between the maximal V_{OC} and the acceleration in the X and Y directions, respectively.

the maximal applied voltage on the load capacitance for each channel can be described by:

$$U_{\max} = \frac{Q}{C_0 + C_{load}} \quad (3)$$

Figure 4a,c shows the measured dual-channel applied voltages when the PTFE layer slides in the X and Y directions, respectively, for 6 different load capacitances from 200 pF to 10 nF at a sliding displacement of 70 mm and an acceleration rate of ±1 m s^{-2}. The maximal applied voltages from both pairs of electrodes decrease with increasing load capacitance, which is shown in Figure 4b,d. The measurement results accord well with Equation (3), which indicates that the smaller the load capacitance, the larger the driving voltage that is applied on the device. As many piezoelectric and electrostatic micro-actuators have a very small capacitance, planar sliding TENGs would be very suitable for actuating these types of devices.

Based on our planar sliding TENG, an active piezoelectric micro-actuator with two piezoelectric bimorphs was developed for two-dimensional optical direction modulation, as schematically illustrated in **Figure 5**a. The two piezoelectric bimorphs were orthogonally positioned and driven by the dual-channel output voltages of the TENG. Each of the piezoelectric bimorphs was fixed on one end as a micro-cantilever structure and subject to a bending deformation by the applied voltage. The structure and principle of the piezoelectric bimorph is detailed in the Supporting Information, as well as the relationship between the deflection angle θ at the free end and the applied voltage U_{load} at small deformation, which can be described by:[24]

$$\theta = \frac{3d_{31} \cdot U_{load} \cdot l}{2h^2} \quad (4)$$

where d_{31} and l are the piezoelectric constant and length of the piezoelectric bimorph, respectively, and h is the thickness of the unimorph in the piezoelectric bimorph. Figure 5b shows the calibration of the piezoelectric bimorph with a capacitance of 392 pF, which accords well with Equation (4) and demonstrates a good linear mechanical output.

As shown in Figure 5a, the laser beam is reflected by both the piezoelectric bimorphs in sequence and received by the screen as a light-spot. The output voltage from one channel is used to drive the first piezoelectric bimorph into a bending deformation, which causes the light spot to move in the OA direction. Whereas the output voltage from the other channel is used to drive the second piezoelectric bimorph into a bending deformation, which causes the light spot to move in the OB direction. Therefore, the dual-channel output voltages can modulate the optical direction two-dimensionally. The relationships between the moving distances of the light-spot on the screen and the sliding displacements L_x and L_y of the PTFE layer were analyzed in the Supporting Information, and can be described by:

$$S_{OA} = \frac{3d_{31} \cdot Q \cdot l \cdot D}{(C_0 + C_{bimorph}) \cdot h^2 L} \cdot L_x \quad (5)$$

$$S_{OB} = \frac{3d_{31} \cdot Q \cdot l \cdot D}{(C_0 + C_{bimorph}) \cdot h^2 L} \cdot L_y \quad (6)$$

© 2014 WILEY-VCH Verlag GmbH & Co. KGaA, Weinheim

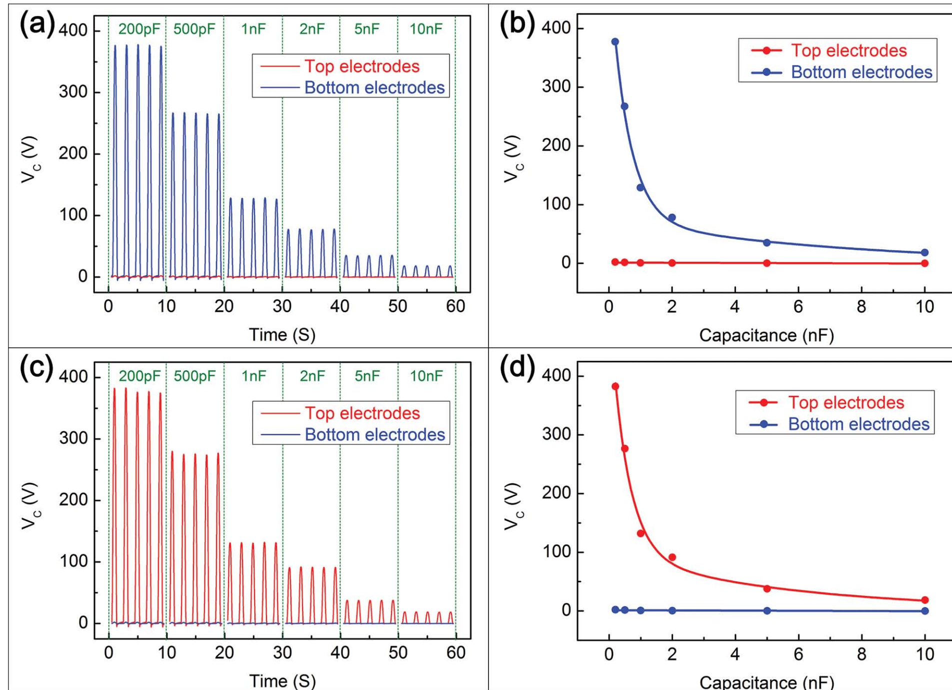

Figure 4. Influence of the load capacitances on the output voltages. a,c) The applied voltages for 6 different load capacitances from 200 pF to 10 nF when the PTFE layer slides in the *X* and *Y* directions, respectively, at a sliding displacement of 70 mm and an acceleration rate of ±1 m s^{-2}. b,d) The relationship between the maximal applied voltages and the load capacitances when the PTFE layer slides in the *X* and *Y* direction, respectively.

where S_{OA} and S_{OB} are the moving distances of the light spot in the OA and OB directions, respectively, D is the distance to the screen and $C_{bimorph}$ is the capacitance of the piezoelectric bimorph.

Figure 5c,d shows the dependence of the moving distances of the light-spot on the screen 1.0 meters away of the sliding displacements of the PTFE layer in the *X* and *Y* directions, respectively, at the acceleration rate of ±1 m s^{-2}. The moving distances in the OA and OB directions have an independent and linear relationship to the sliding displacements in the *X* and *Y* direction, respectively, which demonstrates a good mechanical transmission of the active piezoelectric micro-actuator. The sensitivities were 0.250 for the OA direction and 0.247 for the OB direction, respectively. Figure 5e,f shows the light-spot moving ranges on the screen for sliding of the PTFE layer over 70 mm in the *X* and *Y* directions, respectively, at 6 different sliding accelerations from 0.1 to 4 m s^{-2}. The light-spot moving ranges in both directions were almost constant with increasing sliding speed, which indicates that the sliding speed has little influence on the optical direction modulation. Therefore, the active piezoelectric micro-actuator based on our planar sliding TENG and two piezoelectric bimorphs has successfully realized a two-dimensional optical direction modulation.

Based on the planar sliding TENG, an active electrostatic micro-actuator with two dynamic variable infrared optical attenuators for double-channel optical power modulation was also developed, as schematically illustrated in **Figure 6**a. As the usual MEMS variable optical attenuators,[25,26] the optical attenuation can be adjusted by the applied voltage with this device. Figure 6b shows the calibration of the MEMS optical attenuator with 11 pF capacitance, which indicates that the insertion loss is –0.5 dB and the attenuation range is 28.5 dB from 0 to 5 V. The two optical attenuators were driven by the dual-channel output voltages of the TENG. A capacitance of 47 nF was connected in parallel for each channel to adjust the output voltage to within the working voltage range of the optical attenuator. Two infrared laser beams were transmitted to the attenuators by the fibers and received by the Watt meters.

Figure 6c,d shows the dependence of the attenuation for the two channels on the displacements of the PTFE layer in the *X* and *Y* directions, respectively, at the acceleration rate of ±1 m s^{-2}. The attenuation in each channel could be adjusted independently by the sliding displacement in the *X* and *Y* direction, respectively. The attenuation curves are very similar to the calibrated characteristics in Figure 6b, which also demonstrate a good mechanical transmission of the active electrostatic micro-actuator. The attenuation range was 25.9 dB for attenuator I and 24.9 dB for attenuator II. Figure 6e,f shows the attenuation ranges with the PTFE layer sliding 70 mm in the *X* and *Y* directions, respectively, at 6 different sliding accelerations ranging from 0.1 to 4 m s^{-2}. The attenuations in both channels were almost constant with increasing sliding speed, which indicates that the sliding speed has little influence on the optical power modulation. Therefore, an active electrostatic micro-actuator based on the planar sliding TENG and two MEMS optical attenuators has successfully been realized for dual-channel optical power modulation.

In summary, we present a planar sliding triboelectric nanogenerator with two pairs of orthogonal electrodes and

© 2014 WILEY-VCH Verlag GmbH & Co. KGaA, Weinheim

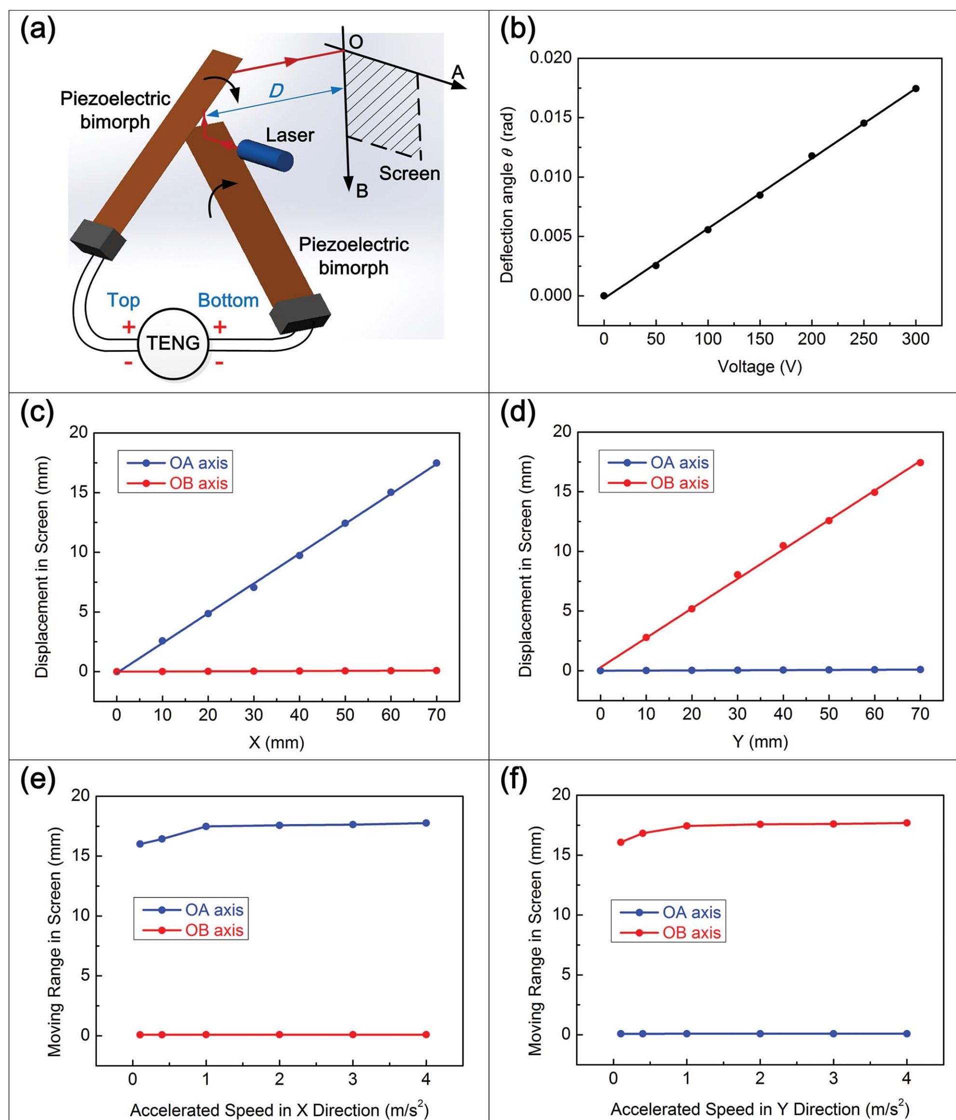

Figure 5. Structure and performances of the active piezoelectric actuator for two-dimensional direction modulation. a) The structure of the active two-dimensional direction modulator with two orthogonal positioned piezoelectric bimorphs and the planar sliding TENG. b) Calibration of the piezoelectric bimorph with 392 pF capacitance. c,d) The dependence of the planar displacements of the light-spot on a screen 1.0 meters away on the displacements of the PTFE layer in the *X* and *Y* directions, respectively, at an acceleration rate of ± 1 m s^{-2}, respectively. The sensitivity was 0.250 for the *X* direction and 0.247 for the *Y* direction. e,f) The light-spot moving range at different acceleration rates of the PTFE layer sliding over 70 mm in the *X* and *Y* directions, respectively.

dual-channel output voltages, which are used for driving the capacitive micro-actuators. The dual-channel output voltages were independently proportional to the sliding displacements of the triboelectric-layer in the *X* and *Y* directions, respectively. The smaller the load capacitance actuated by the TENG, the larger the applied voltage on the capacitive device. Based on this planar sliding TENG, active piezoelectric and electrostatic micro-actuators were developed for two-dimensional optical direction and dual-channel power modulation, respectively. The modulation effects were dependent on the sliding displacements in the plane of the triboelectric layer, however, the sliding speeds had little effect. This work presents for the first time active micro-actuators driven by mechanical energy without the need for external power or mechanical joints. We have as such demonstrated the great capabilities of TENGs for actuating micromechanics and their broad prospects for independent and sustainable self-powered MEMS/NEMS. Together with tribotronics, these active micro-actuators have opened up new applications for TENGs in triboelectric-voltage-controlled devices.

Supporting Information

Supporting Information is available from the Wiley Online Library or from the author.

© 2014 WILEY-VCH Verlag GmbH & Co. KGaA, Weinheim

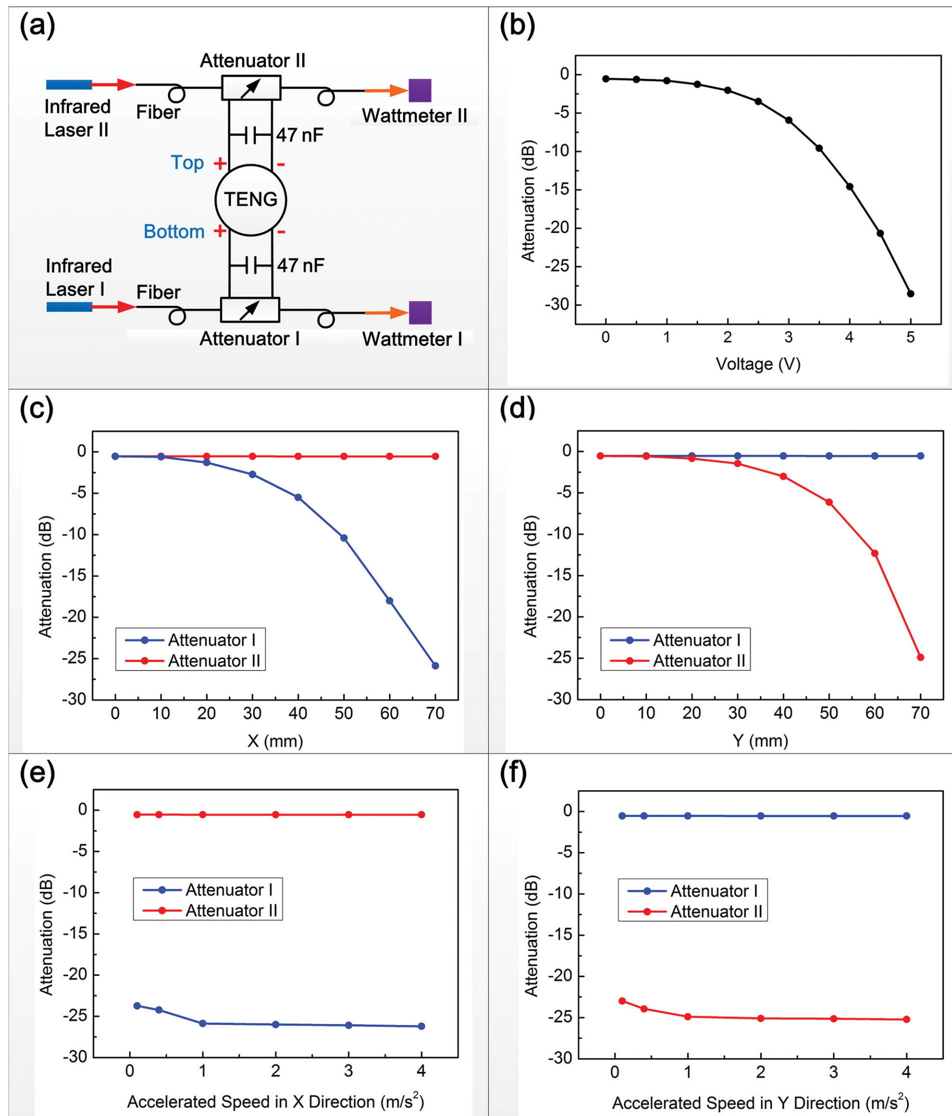

Figure 6. Structure and performances of the active electrostatic actuator for double-channel power modulation. a) The structure of the active double-channel dynamic variable infrared optical attenuator based on an electrostatic MEMS mirror and the planar sliding TENG. b) Calibration of the MEMS optical attenuator with 11 pF capacitance. c,d) The dependence of the attenuation for the two channels on the displacements of the PTFE layer in the *X* and *Y* directions, respectively, at an acceleration rate of ± 1 m s^{-2}. The attenuation range was 25.9 dB for attenuator I and 24.9 dB for attenuator II. e,f) The attenuation ranges at different acceleration rates for the PTFE layer sliding 70 mm in the *X* and *Y* direction, respectively.

Acknowledgements

The project is supported by the National Natural Science Foundation of China (Grant No. 51475099, Grant No. 51432005), the "thousands talents" program for the pioneer researcher and his innovation team, China, and the Beijing Municipal Science & Technology Commission (Z131100006013004, Z131100006013005). We also thank Tao Zhou and Limin Zhang for the discussions.

Received: September 16, 2014
Published online: November 27, 2014

[1] Z. L. Wang, *Sci. Am.* **2008**, *298*, 82.
[2] Z. L. Wang, W. Z. Wu, *Angew. Chem. Int. Ed.* **2012**, *51*, 11700.
[3] Z. L. Wang, *Adv. Mater.* **2012**, *24*, 280.
[4] Y. Suzuki, D. Miki, M. Edamoto, M. Honzumi, *J. Micromech. Microeng.* **2010**, *20*, 104002.
[5] H. Liu, C. Lee, T. Kobayashi, C. J. Tay, C. Quan, *Sensors Actuators A: Phys.* **2012**, *186*, 242.
[6] M. Han, Q. Yuan, X. Sun, H. Zhang, *J. Microelectromech. Systems* **2014**, *23*, 204.
[7] L. Wang, F. G. Yuan, *Smart Mater. Struct.* **2008**, *17*, 045009.
[8] F. R. Fan, Z. Q. Tian, Z. L. Wang, *Nano Energy* **2012**, *1*, 328.
[9] C. Zhang, T. Zhou, W. Tang, C. B. Han, L. M. Zhang, Z. L. Wang, *Adv. Energy Mater.* **2014**, *4*, 1301798.
[10] C. B. Han, C. Zhang, W. Tang, X. H. Li, Z. L. Wang, *Nano Res.* **2014**, DOI: 10.1007/s12274–014–0555–3.
[11] C. B. Han, W. M. Du, C. Zhang, W. Tang, L. M. Zhang, Z. L. Wang, *Nano Energy* **2014**, *6*, 59.
[12] T. Zhou, C. Zhang, C. B. Han, F. R. Fan, W. Tang, Z. L. Wang, *ACS Appl. Mater. Interfaces* **2014**, *6*, 14695.

© 2014 WILEY-VCH Verlag GmbH & Co. KGaA, Weinheim

COMMUNICATION

[13] C. B. Han, C. Zhang, X. H. Li, L. M. Zhang, T. Zhou, W. G. Hu, Z. L. Wang, *Nano Energy* **2014**, *9*, 325.
[14] L. M. Zhang, F. Xue, W. M. Du, C. B. Han, C. Zhang, Z. L. Wang, *Nano Res.* **2014**, *7*, 1215.
[15] Z. L. Wang, *ACS Nano* **2013**, *7*, 9533.
[16] C. Zhang, W. Tang, C. B. Han, F. R. Fan, Z. L. Wang, *Adv. Mater.* **2014**, *26*, 3580.
[17] F. R. Fan, W. Tang, Y. Yao, J. J. Luo, C. Zhang, Z. L. Wang, *Nanotechnol.* **2014**, *25*, 135402.
[18] G. Zhu, J. Chen, T. Zhang, Q. Jing, Z. L. Wang, *Nat. Commun.* **2014**, DOI: 10.1038/ncomms4426.
[19] W. Tang, T. Zhou, C. Zhang, F. R. Fan, C. B. Han, Z. L. Wang, *Nanotechnol.* **2014**, *25*, 225402.
[20] W. Tang, C. B. Han, C. Zhang, Z. L. Wang, *Nano Energy* **2014**, *9*, 121.
[21] W. Tang, C. Zhang, C. B. Han, Z. L. Wang, *Adv. Funct. Mater.* **2014**, *24*, 6684.
[22] C. Zhang, W. Tang, L. M. Zhang, C. B. Han, Z. L. Wang, *ACS Nano* **2014**, *8*, 8702.
[23] C. B. Han, C. Zhang, J. J. Tian, X. H. Li, L. M. Zhang, Z. Li, Z. L. Wang, *Nano Res.* **2014**, DOI: 10.1007/s12274-014-0634-5.
[24] C. Poizat, A. Benjeddou, *Comput. Struct.* **2006**, *84*, 1426.
[25] K. Isamoto, K. Kato, A. Morosawa, C. Chong, H. Fujita, H. Toshiyoshi, *IEEE J. Sel. Top. Quant.* **2004**, *10*, 570.
[26] H. Cai, X. M. Zhang, C. Lu, A. Q. Liu, E. H. Khoo, *IEEE Photonics Technol. Lett.* **2005**, *17*, 402.

© 2014 WILEY-VCH Verlag GmbH & Co. KGaA, Weinheim